Modular Design of Redox-Responsive Stabilizers for Nanocrystals

Kathrin Fuhrmann, Anna Połomska, Carmen Aeberli, Bastien Castagner, Marc A. Gauthier, and Jean-Christophe Leroux*

Institute of Pharmaceutical Sciences, Department of Chemistry and Applied Biosciences, Swiss Federal Institute of Technology Zurich (ETH Zürich), Wolfgang-Pauli-Straße 10, 8093 Zurich, Switzerland

ABSTRACT Many potent drugs are difficult to administer intravenously due to poor aqueous solubility. A common approach for addressing this issue is to process them into colloidal dispersions known as "nanocrystals" (NCs). However, NCs possess high-energy surfaces that must be stabilized with surfactants to prevent aggregation. An optimal surfactant should have high affinity for the nanocrystal's surface to stabilize it, but may also include a trigger mechanism that could offer the possibility of altering size distribution and uptake of the NC. This study presents a modular and systematic strategy for optimizing the affinity of polymeric stabilizers for drug nanocrystals both before and after oxidation (*i.e.*, the selected trigger), thus allowing for the optimal responsiveness for a given application to be identified. A library of 10 redox-responsive polymer stabilizers was prepared by postpolymerization modification, using the thiol−yne reaction, of two parent block copolymers. The stabilizing potential of these polymers for paclitaxel NCs is presented as well as the influence of oxidation on size and dissolution following exposure to reactive oxygen species (ROS), which are strongly associated with chronic inflammation and cancer. Owing to the versatility of postpolymerization modification, this contribution provides general tools for preparing triggered-sheddable stabilizing coatings for nanoparticles.

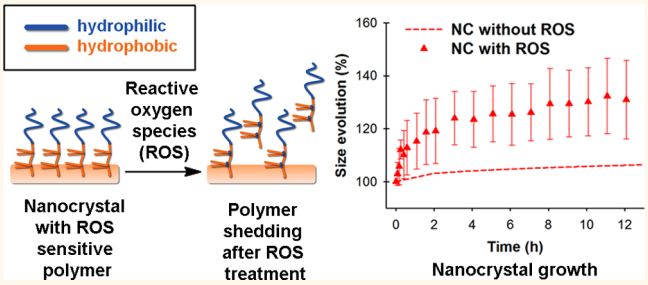

KEYWORDS: thiol−yne · postpolymerization modification · nanocrystals · nanoparticles · paclitaxel · polyester · reactive oxygen species

Many key features of nanoparticles, such as size stability, propensity to aggregation, photonic properties, dissolution profiles, interactions with biomolecules, and circulation lifetime, intrinsically depend on the efficacy of stabilizing agents to mask their surface.[1,2] Correspondingly, much work has been devoted to the development of stabilizing agents for drug nanocrystals (NCs), quantum dots, metal nanoparticles, *etc.*[3−5] Interestingly, developing methods for spatiotemporally destabilizing nanoparticles has received much less attention,[6−9] despite the fact that this property may have applications in imaging and drug delivery. Triggered destabilization can, in principle, be achieved by developing functional stabilizers whose properties change in response to a local endogenous stimulus. However, designing such a system requires that the dynamic noncovalent interactions between the stabilizer in both the original and "triggered" state be carefully balanced to the surface chemistry of the nanoparticle, which can vary broadly. This poses several synthetic and developmental challenges that have impeded the design of tailored responsive stabilizers.

This study presents a simple strategy for systematically adjusting the affinity of polymeric stabilizers for nanoparticles and which simultaneously introduces chemical groups that are sensitive to endogenous oxidants, such as reactive oxygen species (ROS). ROS are strongly associated with chronic inflammation and cancer,[10] and, owing to their short lifetime, their action is limited to these locations. ROS are notably associated with tumor tissues where hypoxic stress causes ROS-mediated signaling.[11] This endogenous stimulus is increasingly being investigated as a means of triggering the response of smart polymeric systems. Examples include nanoparticles made of polymeric (aryl) boronic esters,[12,13] of poly(propylene sulfide),[14−16]

* Address correspondence to jleroux@ethz.ch.

Received for review July 19, 2013 and accepted August 22, 2013.

Published online August 22, 2013
10.1021/nn4037317

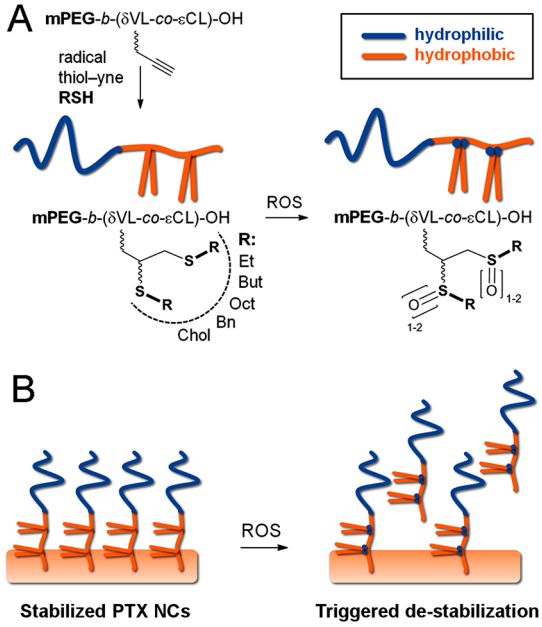

Figure 1. (A) Synthesis of a library of 10 oxidation-sensitive polymeric stabilizers by thiol–yne postpolymerization modification. (B) Oxidation of the stabilizer by endogenous oxidants (*e.g.*, ROS) triggers desorption from the surface of NCs, leading to destabilization.

or of cross-linked oligo(proline).[17] In the current study, paclitaxel (PTX) NCs were selected as a model for demonstrating how ROS-sensitive polymeric stabilizers can be systematically and rationally tuned to achieve the best compromise between stability prior to oxidation and subsequent responsiveness upon exposure to ROS. PTX NCs have already been examined for their therapeutic potential in treating cancer and thus represent a pharmaceutically relevant system. Notably, the size of PTX NCs is expected to strongly depend on their stabilizing coating, and triggered destabilization may be of interest for promoting cellular uptake.[9,18]

A library of 10 redox-responsive amphiphilic block copolymer stabilizers was prepared from two parent block copolymers (methoxy polyethylene glycol-*b*-[α-propargyl-δ-valerolactone-*co*-ε-caprolactone] (mPEG-*b*-[PδVL-*co*-εCL]); Figure 1A) by postpolymerization modification using the thiol–yne reaction. Postpolymerization modification is a powerful tool for systematically altering the functionality of polymers without influencing chain length or chain length distribution.[19] The radical thiol–yne reaction is well established as a mild, efficient, and functional group tolerant reaction, which conforms to the criteria of "click" chemistry.[20] This reaction was used to systematically alter the polarity of the polyester block by grafting different hydrophobic thiols, while the two thioether linkages produced at each PδVL repeat unit render this block sensitive to oxidation by ROS (Figure 1). Oxidation of the thioether to a sulfoxide or sulfone significantly alters the polarity of the hydrophobic block,[21] which may in turn cause desorption from the surface of the NC. The influence of the nature of the hydrophobic thiol agent grafted to the polymer on its stabilizing potential for PTX NCs is reported herein as well as the response of stabilized PTX NCs toward oxidizing conditions.

TABLE 1. Characteristics of Stabilizers Examined in This Study

	composition	R	$M_{n,SEC}$(kDa)[a]	M_w/M_n	thiol–yne coupling (%)[b]
1	$P\delta VL_2\ \varepsilon CL_3$		2.6	1.1	
2	$P\delta VL_2\ \varepsilon CL_3$	Et	2.8	1.3	100
3	$P\delta VL_2\ \varepsilon CL_3$	Bu	2.8	1.3	100
4	$P\delta VL_2\ \varepsilon CL_3$	Oct	3.3	1.5	100
5	$P\delta VL_2\ \varepsilon CL_3$	Bn	3.6	1.8	90
6	$P\delta VL_2\ \varepsilon CL_3$	Chol	3.9	1.9	100
7	$P\delta VL_4$		2.8	1.1	
8	$P\delta VL_4$	Et	2.8	1.4	100
9	$P\delta VL_4$	Bu	3.1	1.4	100
10	$P\delta VL_4$	Oct	3.8	1.8	100[c]
11	$P\delta VL_4$	Bn	3.6	2.4	95
12	$P\delta VL_4$	Chol	2.9	1.3	100
13	εCL_5		2.6	1.1	
14	PSO_9		2.7	1.1	

[a] In THF. [b] By ^{1}H NMR spectroscopy. [c] By MALDI-TOF MS. Abbreviations: ethyl (Et), *n*-butyl (Bu), *n*-octyl (Oct), benzyl (Bn), and cholesteryl (Chol).

RESULTS AND DISCUSSION

Stabilizer Design and Synthesis. As illustrated in Figure 1A, a block copolymer structure was chosen as a template for the preparation of redox-responsive polymeric stabilizers. Two parent copolymers bearing alkynyl groups in the hydrophobic block were prepared by cationic ring-opening polymerization of mixtures of PδVL and εCL from a mPEG initiator (**1** and **7** in Table 1). This polymerization approach is advantageous for producing polymers for pharmaceutical applications owing to the absence of transition metal catalysts.[22] mPEG was selected as hydrophilic polymer segment to prevent NC agglomeration by masking their high-energy surfaces and to convey "stealth-like" properties to the NCs.[23−25] The number of repeat units in the polyester block was targeted to be low (*ca.* 4−5) so that affinity to the NC surface would not be too strong to prevent desorption upon oxidation and so that individual oxidation events within this short block would stand a chance of significantly influencing the overall polarity of the chain (*i.e.*, for responsiveness). **1** and **7** possessed narrow molecular weight distributions (Figure 2A), and analysis of their ^{1}H NMR spectra (Figure 2B, Supplementary Figures S1 and S2) allowed for the accurate determination of the final composition of the short hydrophobic segment (Table 1).

Postpolymerization modification of **1** and **7** by radical thiol–yne coupling using various alkyl, aromatic, and multicyclic thiols led to the straightforward and efficient preparation of the library of polymeric

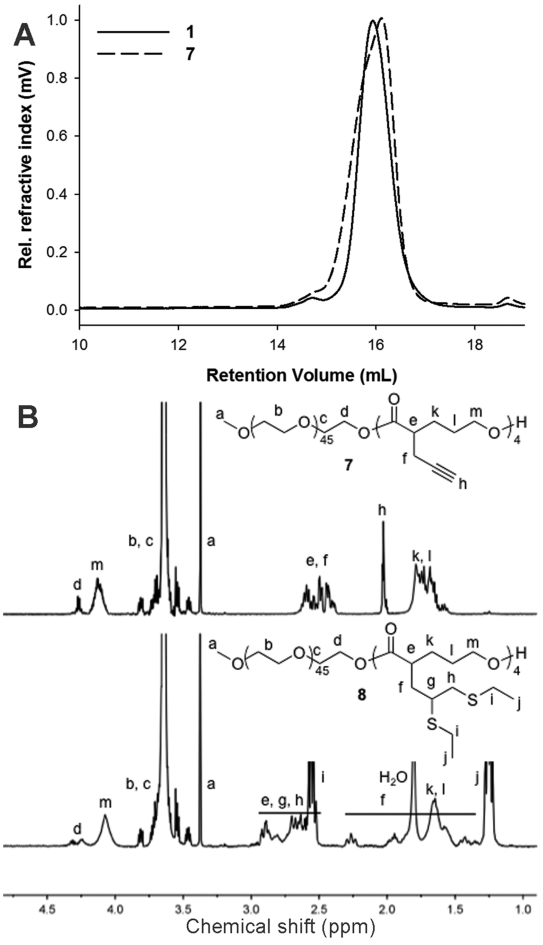

Figure 2. Polymer library synthesis by postpolymerization modification. (A) SEC traces of parent polymers 1 and 7 in THF. (B) Representative ^{1}H NMR spectra of 7 and 8 demonstrating quantitative functionalization by thiol−yne coupling. Assignments based on the ^{1}H−^{1}H correlation spectrum of 8 (Supplementary Figure S8).

stabilizers **2**−**6** and **8**−**12** (Table 1) with systematically different number and nature of side chains (Figure 1A). Quantitative grafting of all thiols except benzyl mercaptane was achieved in less than 30 min as determined by ^{1}H NMR spectroscopy (Figure 2B). For **5** and **11**, small peaks at 5.4 and 5.9 ppm corresponding to the monosubstituted vinyl sulfide were observed (Supplementary Figures S3 and S4). For **10**, which bore eight octyl units, integration of the ^{1}H NMR spectrum did not match expectations, although peaks associated with monosubstituted vinyl sulfide were not observed (Supplementary Figure S5). Consequently, matrix-assisted laser desorption ionization time-of-flight mass spectrometry was used to verify complete functionalization of the polymer. The latter showed a multiple peak distribution with mass differences of about 430.29, which corresponds to one δ-valerolactone monomer conjugated with two octanethiols. In addition, FTIR spectroscopy revealed complete disappearance of the characteristic stretching vibration of the alkynyl group at 3270 cm^{-1} following thiol−yne

TABLE 2. Characteristics of Stabilized PTX NCs Examined in This Study

stab.	R	PTX conc. (mg/mL)[a]	size (nm)[a]	PDI[b]	PTX content (wt %)	$L/2R_g$[c]
2	Et	0.82	180	0.234	77	0.40
3	Bu	0.60	285	0.255	79	0.43
4	Oct	0.29	189	0.211	77	0.43
5	Bn	0.42	298	0.219	78	0.45
8	Et	0.77	232	0.206	76	0.42
9	Bu	0.54	193	0.218	73	0.37
10	Oct	0.19	176	0.133	69	0.32
13		0.91	136	0.137	82	0.41
14		0.64	229	0.190	74	0.41

[a] After centrifugation. [b] Polydispersity index. [c] L is the average mean distance between mPEG chains; R_g is the radius of gyration of "free" mPEG in aqueous solution; $L/2R_g > 1$ mPEG is well separated and in mushroom conformation, <1 mPEG in brush conformation, <0.5−0.7 enhanced protein resistance regime.[28]

functionalization (Supplementary Figure S6). Analytical size-exclusion chromatography in THF showed in most cases a monomodal molecular weight distribution, although as the hydrophobicity (and bulk) of the polyester block increased, the chromatograms became less well-defined, likely due to potential enthalpic interaction with the stationary phase of the column (Supplementary Figure S7).

NC Production and Stability. PTX NCs were produced by wet-milling in the presence of **2**−**6** and **8**−**12** as well as with mPEG-*b*-εCL (**13**) or mPEG-*b*-poly(styrene oxide) (mPEG-*b*-PSO, **14**), which are unbranched aliphatic and aromatic controls, respectively. Overall, 14 polymers were investigated for their ability to sterically stabilize PTX NCs. With the exception of **6**, **11**, and **12**, wet-milling of PTX for 18−48 h led to the production of NCs with mean diameters around 200 nm, as determined by dynamic light scattering, which is in accordance with requirements for systemic administration. The size and shape of particles obtained by wet-milling were consistent with values reported for PTX NCs elsewhere.[26,27] NCs were subjected to a short centrifugation step to remove larger aggregates, and then PTX concentration was measured by high-performance liquid chromatography (Table 2). PTX recovery was lower with increasing hydrophobicity of the polymer, which indicates inefficient milling in cases where self-aggregation is favored *versus* the interaction of the polymer with the NC surface. While the polymers bearing the pendant cholesteryl and benzyl units were poorly soluble and inefficient stabilizers for PTX NCs, the ability to quantitatively introduce complex and bulky groups such as these by the thiol−yne reaction demonstrates the versatility of the chemistry employed. Inefficient stabilization of NCs observed using **6**, **11**, and **12** may be related to the presence of branching within the hydrophobic segment. Indeed polymer functionality can be broadly tuned using the extensive list of commercially available thiol agents.

The characteristic needle-like shape of PTX NCs was observed by transmission electron microscopy (TEM)

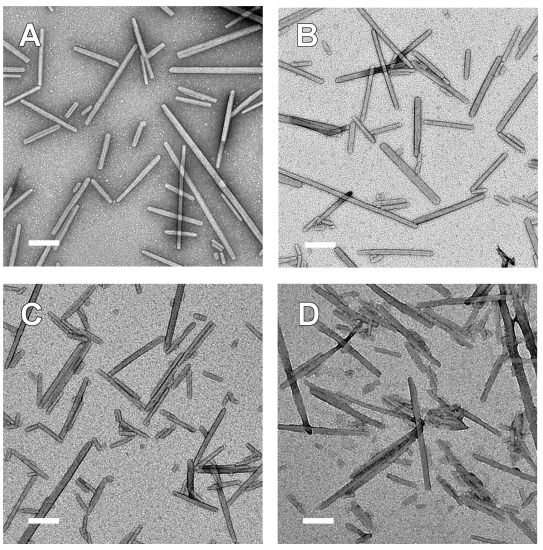

Figure 3. Representative transmission electron micrographs of PTX NCs stabilized with (A) 3, (B) 4, (C) 8, and (D) 9. Scale bars represent 200 nm.

for all stabilizers (examples in Figure 3). Under the simplification that the NCs are cylindrical, the average specific surface area of the NCs was determined from these images. This, in combination with drug content determined by ^{1}H NMR spectroscopy, allowed for the calculation of the amount of polymer per surface area of the NC, which can be expressed as L, the average mean distance between mPEG chains. According to the geometric model of Pasche *et al.*,[28] the ratio $L/2R_g$ (R_g being the radius of gyration for free mPEG) was calculated to provide an indication of the packing structure of the stabilizer on the NC (Table 2). An $L/2R_g$ higher than 1 suggests that mPEG is well separated and in mushroom conformation, while an $L/2R_g$ below 1 indicates brush conformation. mPEG-modified surfaces with $L/2R_g$ below 0.5−0.7 have been reported to efficiently reduce protein adsorption.[28] On the basis of this model, all stabilizers on the surface of PTX NCs were within a dense brush regime ($L/2R_g$ ranges from 0.32 to 0.45; see Table 2), suggesting intimate contact and interaction between neighboring polymer chains. While stabilizer surface density for all polymers was roughly the same, a trend toward increased stabilizer density was observed from **8** to **10** (increasing side-chain length).

Following purification, the stabilized NCs were stored at room temperature (Figure 4), and their size over time was monitored by dynamic light scattering. Compared to the branched polymers, the unbranched aliphatic control **13** was the least efficient stabilizer, pointing to the importance of multiple interactions and intimate contact within the hydrophobic domain. Polymers **2**−**5** (*i.e.*, with four branches) provided improved size stability compared to **13** (Figure 4C). Increasing the number of branches to eight (polymers **8**−**10**, Figure 4B) led to significant stabilization of the

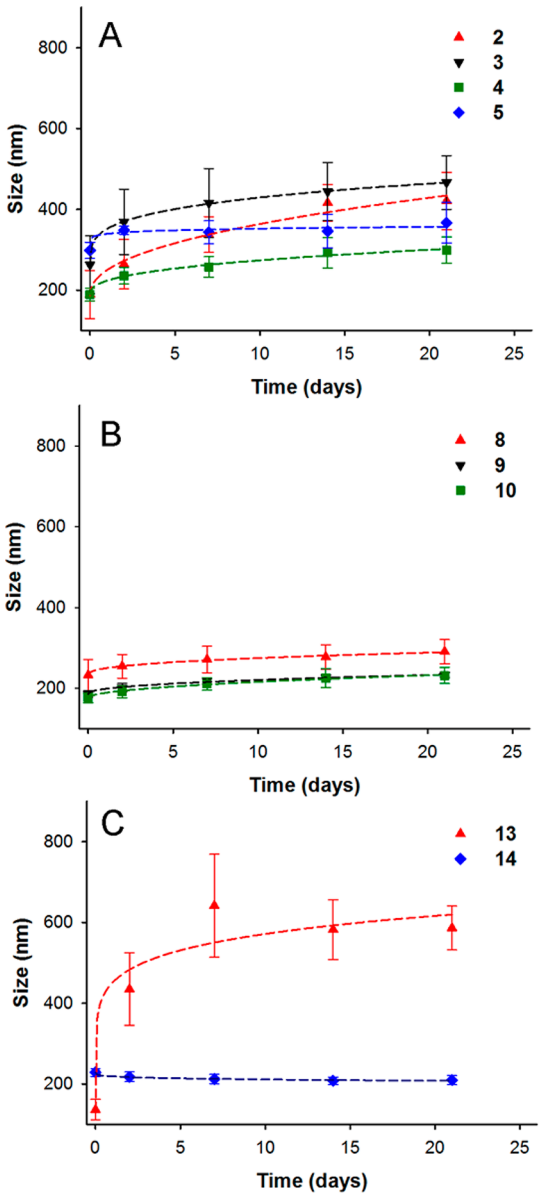

Figure 4. Size stability of PTX NCs stabilized with (A) 2−5, (B) 8−10, and (C) 13 and 14 at room temperature. Values represent mean ± SD (n = 3−6).

NCs over a period of more than 21 days. At 6 °C, little or no evolution in size was observed for any of the stabilized NCs (Supplementary Figure S9), suggesting that the size increase observed at room temperature was due to Ostwald ripening rather than aggregation. It should be noted that the influence of mass transport, which is affected by initial NC size and concentration, on NC stability cannot be discounted, and the relative similarity of these parameters between samples suggests that their effect is secondary to stabilizer chemistry in Figure 4.

Response of PTX NCs to Reactive Oxygen Species. Stabilizers **2**−**6** and **8**−**12** contain on average four and eight thioether bonds per polymer chain, respectively. Oxidation of these groups produces a sulfoxide and

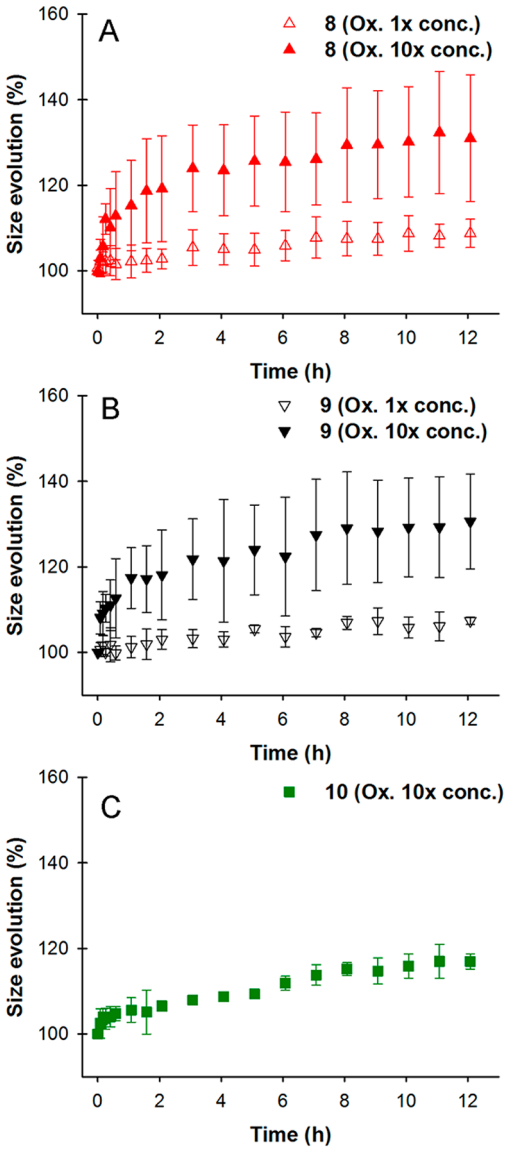

Figure 5. Size stability of PTX NCs stabilized with 8 (A), 9 (B), and 10 (C) after exposure to an oxidizing agent (oxidant concentration: 1×, 0.1 mM H_2O_2/0.01 mM $FeSO_4$; 10×, 1 mM H_2O_2/0.1 mM $FeSO_4$). Data represent mean ± SD, n = 3–4.

ultimately a sulfone.[21] This process is expected to impart a large change of polarity to the hydrophobic block of the stabilizer. For instance, while the thioether side chain of methionine in proteins is one of the most hydrophobic, its sulfoxide/sulfone form is more hydrophilic and bulky, which is used in practice for protein secondary structure characterization by breaking β-sheet assembly.[29,30] As PTX NCs stabilized with **8**–**10** demonstrated excellent size stability (Figure 4B), their response to ROS was investigated. These NC suspensions are characterized by a high drug content (69–82%; see Table 2), which implies that the ROS responsiveness of only a minor component (*i.e.*, the stabilizer) has the potential to trigger the destabilization of a correspondingly large amount of drug. To examine the sensitivity of **8** and **9**, a low concentration of ROS was first examined (100 μM H_2O_2, 10 μM $FeSO_4$). As shown in Figure 5A and B, this concentration did not influence NC stability. However, exposure to an increased oxidizing environment (1 mM H_2O_2, 0.1 mM $FeSO_4$) led to the rapid destabilization of NCs prepared with **8** and **9**. Oxidation of the thioether was monitored by ^{1}H NMR spectroscopy analysis of the fraction of **8** that was shed from the NC. Examination of the ^{1}H–^{1}H correlation spectrum revealed the appearance of a new signal consistent with an ethylsulfoxide group, at lower field than the corresponding ethylthioether (Supplementary Figure S10), as expected from prior observations from the literature.[31] Overlapping signals in the 1D ^{1}H NMR spectrum do not allow for precise quantification, as only a low level of oxidation was observed. Semiquantitative analysis suggests that only a single or very few oxidation events within the very short hydrophobic block were able to drive **8** from the surface of the PTX NCs. Thus a greater responsiveness to oxidation in comparison to other thioether-based materials was observed. For the latter, multiple oxidation events are required to significantly alter the polarity of the individual polymer chains. Responsiveness was manifested by a rapid increase in size beginning well within the first hour (Figure 5), which then leveled off thereafter. The size distribution of the NCs also increased to a certain extent after exposure to ROS. TEM images of NCs before and after exposure to ROS suggest that the increased size observed by light scattering could be the result of aggregation, due to exposure of hydrophobic PTX areas (Supplementary Figures S11 and S12). Bearing in mind that this is a closed system, oxidation of **8** produced a shedding of about 20% of the stabilizer from the NC (polymer to drug ratio (w/w) decreased from 0.311 ± 0.014 to 0.251 ± 0.006), suggesting that more shedding may be observed within an open system such as the body. NCs stabilized with **10**, bearing eight pendant octyl chains in its hydrophobic block, showed a much slower and less pronounced response to ROS, likely because the longer hydrophobic alkane chain (octane) provided a stronger anchor to the surface of the NC than the shorter ones (*i.e.*, ethane or butane). These combined results suggest that the change of polarity of the stabilizer's hydrophobic block due to a low level of oxidation events is sufficient to induce desorption from the surface of the NC when the pendant groups are short and when the concentration of oxidant is sufficiently high. Exposure to ROS did not significantly influence the release kinetics of PTX from stabilized NCs, which points to the absence of deleterious effects of the oxidation reaction on the NC itself (Supplementary Figure S13).

Sensitivity and Responsiveness Compared to Other ROS-Sensitive Systems. In contrast to other ROS-sensitive drug delivery systems reported in the literature, the stabilized NCs presented herein represent the first example of a core–shell system in which the redox

sensitivity of the shell is designed to release the "insensitive" bulk. As a consequence, ROS-sensitive stabilized NCs stand to respond faster and have the potential to be more sensitive to oxidation than bulk-type systems, for which the oxidation process is slow due to diffusion phenomena, swelling, erosion, *etc*. Indeed, other bulk thioether-based systems have shown to respond over a period of a couple days to very high concentrations of H_2O_2 (5−10 vol %).[16] For instance, Mahmoud *et al*. have reported the release of a dye from thioether-containing particles to occur over 1 day upon exposure to 100 mM H_2O_2.[32] Indeed, it should be noted that Allen *et al*. have recently shown rapid (<10 min) dye release from thioether-containing particles in response to 25−2000 ppm sodium hypochlorite or ROS generated by enzymatic processing of H_2O_2.[15] This study provides an indication that thioether bonds can be very sensitive to other endogenous and potentially more reactive ROS than H_2O_2 and that existing oxidants can be potentiated with enzymes. Interestingly, Almutairi and co-workers have recently reported that polymers bearing aryl boronic ester protecting groups were substantially more sensitive than thioethers to oxidation. Indeed, concentrations of H_2O_2 as low as 100 μM led to polymer backbone degradation and release of about 50% of cargo within 24 h.[12] The system reported in our work is sensitive to oxidant concentrations that are higher than that in the aforementioned studies. However, the reaction was relatively fast (in under 2 h), making the system suitable to target regions with high/moderate ROS concentrations with lower chances of off-target effects (due to oxidation in low ROS concentration regions).

CONCLUSIONS

This study demonstrates that postpolymerization modification *via* the thiol−yne reaction is a powerful tool for rapidly, rationally, and systematically preparing ROS-responsive biodegradable polymeric stabilizers for NCs. Achieving a fine balance between stabilization of the NCs and observing a tangible and rapid response upon oxidation was possible using this approach. The prepared NCs were sensitive to oxidation, and, in the case of PTX, this phenomenon may be self-amplifying due to the known triggering of ROS production in PTX-treated cells.[33,34] This paves the way for the design of ROS-sensitive systems based on nanoparticles and drug NCs and offers many opportunities in the biotechnological field for location-specific shedding of stabilizers, which can be used for imaging[35−37] or for improving cellular uptake.[18,38] While hydrophobic thiols were used herein for affinity with the hydrophobic surface of PTX NCs, the extensive list of other commercially available (and hydrophilic) thiols renders this a universal approach for preparing libraries of polymeric surfactants with precisely the same number of repeat units for the reversible stabilization of drug NCs and potentially other classes of nanoparticles such as quantum dots and gold nanoparticles, for which aggregation strongly influences their photonic properties.[39]

EXPERIMENTAL SECTION

Materials. PTX was obtained from Bioxel Pharma Inc. (Sainte-Foy, QC, Canada), and docetaxel from ScinoPharm Taiwan, Ltd. (Tainan County, Taiwan). Lithium diisopropylamide, δ-valerolactone (δVL), propargyl bromide, hexamethylphosphoramide, ε-caprolactone, ethane-1-thiol, butane-1-thiol, octane-1-thiol, benzyl mercaptane, thiocholesterol, 2,2-dimethoxy-2-phenylacetophenone (99%), pyrene (99%), iron sulfate heptahydrate (>99%, $FeSO_4$), albumin from bovine serum (BSA; ≥96%), and methoxy poly(ethylene glycol) (mPEG; 2 kDa) were purchased from Sigma-Aldrich (Buchs, Switzerland) and used as received. Hydrogen chloride (1 N solution in diethyl ether) was purchased from Chemie Brunschwig AG (Basel, Switzerland), and hydrogen peroxide (30% solution, Perhydrol) from Merck (Altdorf, Switzerland). mPEG-*b*-εCL and mPEG-*b*-PSO were bought from Advanced Polymer Materials (Montreal, QC, Canada). Ultrapure water was obtained from a Barnstead Nanopure system (Thermo Fisher Scientific, Reinach, Switzerland). Dry solvents were taken from a solvent purification system (LC Technology Solutions Inc., Seabrook, NH, USA). δVL and εCL were distilled over calcium hydride under inert atmosphere before use. All other solvents were of highest purity and bought from Sigma-Aldrich (Buchs, Switzerland).

Equipment. ^{1}H NMR spectra were recorded on a Bruker Av400 spectrometer (Bruker BioSpin, Fällanden, Switzerland) operating at 400 MHz for protons. Analytical size-exclusion chromatography (SEC) measurements were performed in THF using a Viscotek TDAmax system (Viscotek, Houston, TX, USA) equipped with a differential refractive index detector. Molecular weights are given relative to narrow PEG standards (PSS Polymer Standards Service GmbH, Mainz, Germany). Separation was achieved using two Viscotek columns (GMHHRM) in series at a flow rate of 1.0 mL·min^{-1} at 45 °C. Particle hydrodynamic diameter was determined by dynamic light scattering using a DelsaNano C particle analyzer (Beckman Coulter, Brea, CA). The cumulants result calculated by the software was used to report the hydrodynamic diameter of the NCs. PTX concentration was determined by HPLC analysis, using an autosampler and pump system (Ultimate 3000, Dionex, Thermo Fisher) equipped with a reversed-phase column (Accucore C_{18} column, 2.6 μm particle size, 100 × 2.1 mm, Thermo Fisher) held in a column oven at 30 °C and a diode array detector (Thermo Fisher Scientific, Reinach, Switzerland). Gradient elution was performed starting with a mix of 40% acetonitrile in water, rising to 70% acetonitrile within 8 min. PTX was detected at 230 nm. A solution of docetaxel in acetonitrile was added as internal standard. FTIR spectra were obtained using ATR geometry on a Spectrum 65 infrared spectrophotometer (Perkin-Elmer, Schwerzenbach, Switzerland).

Synthesis of Polymer Precursors 1. PδVL was synthesized as described elsewhere.[40] In a typical experiment, mPEG (800 mg, 0.4 mmol, 1 equiv) was dried by azeotropic distillation with dry toluene (50 mL) under a flow of nitrogen. The flask was sealed, and the mPEG was dissolved in dry dichloromethane (2 mL). Dry εCL (132.8 μL, 1.2 mmol, 3 equiv) and PδVL (150.5 μL, 1.2 mmol, 3 equiv) were then added using gastight syringes. The polymerization was initiated by the addition of HCl in ether (1.2 mL, 1.2 mmol, 3 equiv) and stirred at room temperature for 24 h. The reaction mixture was then precipitated twice in cold ether, the solvent evaporated *in vacuo*, the residue taken up in water, and the polymer recovered by lyophilization (0.867 g, 80% yield). The synthesis of **7** followed the protocol above with the following quantities: mPEG (1.50 g, 0.75 mmol, 1 equiv), PδVL (564.6 μL, 4.5 mmol, 6 equiv), HCl in ether (1.5 mL, 1.5 mmol,

2 equiv). The fully annotated NMR spectrum of **1** and **7** and the compositions of the polymers can be found in Supplementary Figures S1 and 2 and Table 1, respectively.

Postpolymerization Modification by Radical Thiol−Yne Addition. In a general procedure, **1** (30 mg, 0.0115 mmol, 1 equiv) was dissolved in 100 μL of stabilizer-free tetrahydrofuran. A fresh stock solution of 2,2-dimethoxy-2-phenylacetophenone (0.89 mg, 0.0035 mmol, 5 mol % of thiol compound) in stabilizer-free tetrahydrofuran (THF) was added (8.9 μL) to the polymer solution in a quartz cuvette. After addition of the thiol compound (6 or 12 equiv for modification of **1** and **7**, respectively), the solution was subjected to UV light at 365 nm for 30 min. The solution was then precipitated twice with about 15 volume parts of cold hexane, recovered by centrifugation (unless otherwise stated, see Supporting Information), and dried under a flow of nitrogen. The polymer was dissolved/dispersed in water and lyophilized. Fully annotated ^{1}H NMR spectra of all polymers can be found in Supplementary Figures S14−20.

Preparation of PTX NCs. PTX NCs were produced by wet-milling. In a typical experiment, 2 mL of a 0.5% (w/w) polymer solution in ultrapure water was filtered (0.2 μm pore size) into a 20 mL cylindrical glass vessel containing 10 mg of PTX and 4 mL of zirconium oxide beads (~14.7 g, 0.3 mm in diameter, Union Process, Akron, OH, USA). When the stabilizer was not soluble in water, an aqueous solution was first prepared by micellization following dialysis from an ethanol/water or tetrahydrofuran/water solution. The vessel was closed with a plastic cap, then placed horizontally on a Ratek BTR5 blood tube roller (with custom-modified motor, Labortechnik Fröbel GmbH, Lindau, Germany), and rolled at 220 rpm in a cold room (6 °C) for 18−48 h. After milling, the beads were separated from the suspension by filtration through polyamide sieve fabric (30 μm pores, VWR, Dietikon, Switzerland), and the residue was washed four times with 2 mL of ultrapure water. The suspension was centrifuged at 12000*g* for 6 min to remove larger aggregates.

Imaging of Stabilized PTX NCs. NCs were imaged by TEM. A 4 μL amount of a NC suspension was adsorbed to a glow discharged carbon-coated copper grid for 1 min. After two washings with water, NCs were negatively stained with 2% (w/v) uranyl acetate for 1 min and air-dried after blotting with filter paper. The specimens were examined in a Philips CM12 (tungsten cathode) transmission electron microscope (FEI, Hillsboro, OR, USA) at 100 kV, and images were recorded with a Gatan CCD 794 camera (Gatan Inc., Pleasanton, CA, USA).

Drug to Stabilizer Ratio. NC dispersions were centrifuged at 20000*g* for 90 min at 15 °C. Afterward, the supernatant was carefully and quantitatively removed, and the pellet was dried by lyophilization. The dried pellet was dissolved in deuterated chloroform for ^{1}H NMR spectroscopy. Integration of the aromatic proton signal of PTX at 8.12 ppm *versus* the proton signal of PEG at 3.64 ppm provided an estimate of the drug to stabilizer ratio.

NC Volume and Density of the Stabilizer Coating. Average dimensions of NCs were measured in TEM images. The number of polymer chains ($n_{Polymer}$) per NC can be calculated with eq 1.

$$n_{Polymer} = N_A V \rho (wt_{Polymer}/wt_{PTX})/M_{w\,Polymer} \quad (1)$$

where N_A is Avogadro's constant, V is the average volume of a NC (assumed to be a cylinder), ρ is the density (1.4035 g/mL for PTX dihydrate), $wt_{Polymer}/wt_{PTX}$ is the weight ratio of drug to polymer after centrifugation determined by ^{1}H NMR spectroscopy, and M_w is the weight average molecular weight of the polymer as calculated by ^{1}H NMR spectroscopy.

Dissolution Test. Release of PTX from NCs was tested under sink conditions in a 5% BSA solution, which is expected to be the main solubilizing component for PTX *in vivo*.[41] In a preliminary experiment, the saturation solubility of PTX powder in the test conditions was found to be 0.01 mg·mL^{-1}. A 1 mL Spectra/Por Float-A-Lyzer G2 (MWCO 100 kDa, Sigma-Aldrich, Buchs, Switzerland) was filled by mixing 20 mM phosphate buffer (pH 7.4) containing 10% BSA with NCs in water to yield a final volume of 1 mL containing 0.1 mg·mL^{-1} PTX in 10 mM phosphate buffer (pH 7.4) and 5% BSA. The dialysis device was placed in a 50 mL centrifugation tube containing 45 mL of 10 mM phosphate buffer (pH 7.4) with 5% BSA, on a rotary shaker (~400 rpm) in an incubator at 37 °C. Under these conditions, the maximum PTX concentration was 5 times below its saturation solubility. At selected time points, 30 μL aliquots were taken from inside the dialysis device, prepared for HPLC analysis by addition of 30 μL of internal standard (docetaxel in acetonitrile), and vortexed. After addition of 200 μL of a 0.1 M $ZnSO_4$ solution and 500 μL of acetonitrile the samples were vortexed for 1 min. Following two centrifugation steps of 10 min at 15000*g*, 200 μL of the supernatant was mixed with 100 μL of water, filtered through polyamide (0.2 μm pore size), and analyzed by HPLC as described under Equipment.

Sensitivity to ROS, Dissolution, and Polymer Shedding. NC suspensions were diluted with water to a PTX content of 0.3 mg·mL^{-1}. In the case of NCs formulated with **10** this step was neglected. The NC dilution (0.5 mL) was mixed with Fenton's reagent (H_2O_2/$FeSO_4$ final concentrations of either 1 mM/0.1 mM or 0.1 mM/0.01 mM) directly in a UV cuvette, and size was monitored at 25 °C for 12 h. To determine polymer shedding after oxidation, diluted NC suspensions (0.2 and 0.3 mg·mL^{-1} PTX for polymers **10** and **8**/**9**, respectively) were incubated with 1 mM H_2O_2/0.1 mM $FeSO_4$ for 2 h at room temperature. Then they were treated and analyzed as described under Drug to Stabilizer Ratio. In a further experiment, Fenton's reagent (H_2O_2/$FeSO_4$ final concentration in the mixture 1 mM/0.1 mM) was added to a NC suspension at the beginning of a dissolution test, and then the experiment was conducted as described in the previous section. For the NMR characterization of the shed polymer, a NC suspension stabilized with polymer **8** was incubated with 1 mM H_2O_2 and 0.1 mM $FeSO_4$ for 4 h. The particles were then centrifuged at 20000*g* for 90 min. The supernatant containing shed polymer was collected, lyophylized, and later analyzed by ^{1}H NMR spectroscopy.

Conflict of Interest: The authors declare no competing financial interest.

Acknowledgment. The authors acknowledge A. E. Felber for taking TEM images supported by the Electron Microscopy Center of ETH Zurich (EMEZ) and Prof. I. Werner (pharmaceutical analytics group, IPW, ETH) for kindly providing the infrared spectrophotometer. The authors thank Dr. P. Luciani for her advice on reactive oxygen species and J. D. Schulz for the synthesis of a starting compound. Dr. B. Pfeiffer and L. Betschart are thanked for their assistance with acquisition of the 2D NMR spectra. This work received support from the Swiss National Science Foundation (310030_138342).

Supporting Information Available: Supporting SEC chromatograms, ^{1}H NMR and correlation spectra, MALDI TOF MS and FTIR spectra, additional size stability and dissolution figures. This material is available free of charge *via* the Internet at http://pubs.acs.org.

REFERENCES AND NOTES

1. Budijono, S. J.; Russ, B.; Saad, W.; Adamson, D. H.; Prud'homme, R. K. Block Copolymer Surface Coverage on Nanoparticles. *Colloids Surf. Physicochem. Eng. Aspects* **2010**, *360*, 105–110.
2. Alexis, F.; Pridgen, E.; Molnar, L. K.; Farokhzad, O. C. Factors Affecting the Clearance and Biodistribution of Polymeric Nanoparticles. *Mol. Pharmaceutics* **2008**, *5*, 505–515.
3. Gaucher, G.; Asahina, K.; Wang, J.; Leroux, J.-C. Effect of Poly(N-vinyl-pyrrolidone)-block-Poly(d,l-lactide) as Coating Agent on the Opsonization, Phagocytosis, and Pharmacokinetics of Biodegradable Nanoparticles. *Biomacromolecules* **2009**, *10*, 408–416.
4. Cormode, D. P.; Skajaa, G. O.; Delshad, A.; Parker, N.; Jarzyna, P. A.; Calcagno, C.; Galper, M. W.; Skajaa, T.; Briley-Saebo, K. C.; Bell, H. M.; *et al*. A Versatile and Tunable Coating Strategy Allows Control of Nanocrystal Delivery to Cell Types in the Liver. *Bioconjugate Chem.* **2011**, *22*, 353–361.
5. Schweiger, C.; Pietzonka, C.; Heverhagen, J.; Kissel, T. Novel Magnetic Iron Oxide Nanoparticles Coated with Poly(ethylene imine)-g-Poly(ethylene glycol) for Potential

Biomedical Application: Synthesis, Stability, Cytotoxicity and MR Imaging. *Int. J. Pharm.* **2011**, *408*, 130–137.
6. Romberg, B.; Hennink, W.; Storm, G. Sheddable Coatings for Long-Circulating Nanoparticles. *Pharm. Res.* **2008**, *25*, 55–71.
7. Sankaranarayanan, J.; Mahmoud, E. A.; Kim, G.; Morachis, J. M.; Almutairi, A. Multiresponse Strategies To Modulate Burst Degradation and Release from Nanoparticles. *ACS Nano* **2010**, *4*, 5930–5936.
8. Knipe, J. M.; Peters, J. T.; Peppas, N. A. Theranostic Agents for Intracellular Gene Delivery with Spatiotemporal Imaging. *Nano Today* **2013**, *8*, 21–38.
9. Motion, J. P. M.; Nguyen, J.; Szoka, F. C. Phosphatase-Triggered Fusogenic Liposomes for Cytoplasmic Delivery of Cell-Impermeable Compounds. *Angew. Chem., Int. Ed.* **2012**, *51*, 9047–9051.
10. Fang, J.; Seki, T.; Maeda, H. Therapeutic Strategies by Modulating Oxygen Stress in Cancer and Inflammation. *Adv. Drug Delivery Rev.* **2009**, *61*, 290–302.
11. Preston, T. J.; Abadi, A.; Wilson, L.; Singh, G. Mitochondrial Contributions to Cancer Cell Physiology: Potential for Drug Development. *Adv. Drug Delivery Rev.* **2001**, *49*, 45–61.
12. de Gracia Lux, C.; Joshi-Barr, S.; Nguyen, T.; Mahmoud, E.; Schopf, E.; Fomina, N.; Almutairi, A. Biocompatible Polymeric Nanoparticles Degrade and Release Cargo in Response to Biologically Relevant Levels of Hydrogen Peroxide. *J. Am. Chem. Soc.* **2012**, *134*, 15758–15764.
13. Broaders, K. E.; Grandhe, S.; Fréchet, J. M. J. A Biocompatible Oxidation-Triggered Carrier Polymer with Potential in Therapeutics. *J. Am. Chem. Soc.* **2010**, *133*, 756–758.
14. Khutoryanskiy, V. V.; Tirelli, N. Oxidation-Responsiveness of Nanomaterials for Targeting Inflammatory Reactions. *Pure Appl. Chem.* **2008**, *80*, 1703–1718.
15. Allen, B. L.; Johnson, J. D.; Walker, J. P. Encapsulation and Enzyme-Mediated Release of Molecular Cargo in Polysulfide Nanoparticles. *ACS Nano* **2011**, *5*, 5263–5272.
16. Rehor, A.; Hubbell, J. A.; Tirelli, N. Oxidation-Sensitive Polymeric Nanoparticles. *Langmuir* **2004**, *21*, 411–417.
17. Yu, S. S.; Koblin, R. L.; Zachman, A. L.; Perrien, D. S.; Hofmeister, L. H.; Giorgio, T. D.; Sung, H.-J. Physiologically Relevant Oxidative Degradation of Oligo(proline) Cross-Linked Polymeric Scaffolds. *Biomacromolecules* **2011**, *12*, 4357–4366.
18. Gao, W.; Langer, R.; Farokhzad, O. C. Poly(ethylene glycol) with Observable Shedding. *Angew. Chem., Int. Ed.* **2010**, *49*, 6567–6571.
19. Gauthier, M. A.; Gibson, M. I.; Klok, H.-A. Synthesis of Functional Polymers by Post-Polymerization Modification. *Angew. Chem., Int. Ed.* **2009**, *48*, 48–58.
20. Hoogenboom, R. Thiol−Yne Chemistry: A Powerful Tool for Creating Highly Functional Materials. *Angew. Chem., Int. Ed.* **2010**, *49*, 3415–3417.
21. Napoli, A.; Valentini, M.; Tirelli, N.; Muller, M.; Hubbell, J. A. Oxidation-Responsive Polymeric Vesicles. *Nat. Mater.* **2004**, *3*, 183–189.
22. Kim, M. S.; Seo, K. S.; Khang, G.; Lee, H. B. Ring-Opening Polymerization of ε-Caprolactone by Poly(ethylene glycol) by an Activated Monomer Mechanism. *Macromol. Rapid Commun.* **2005**, *26*, 643–648.
23. Bertrand, N.; Leroux, J.-C. The Journey of a Drug-Carrier in the Body: An Anatomo-Physiological Perspective. *J. Controlled Release* **2012**, *161*, 152–163.
24. Aggarwal, P.; Hall, J. B.; McLeland, C. B.; Dobrovolskaia, M. A.; McNeil, S. E. Nanoparticle Interaction with Plasma Proteins as it Relates to Particle Biodistribution, Biocompatibility and Therapeutic Efficacy. *Adv. Drug Delivery Rev.* **2009**, *61*, 428–437.
25. Torchilin, V. P. Multifunctional Nanocarriers. *Adv. Drug Delivery Rev.* **2006**, *58*, 1532–1555.
26. Cerdeira, A. M.; Mazzotti, M.; Gander, B. Miconazole Nanosuspensions: Influence of Formulation Variables on Particle Size Reduction and Physical Stability. *Int. J. Pharm.* **2010**, *396*, 210–218.
27. Van Eerdenbrugh, B.; Vermant, J.; Martens, J. A.; Froyen, L.; Humbeeck, J. V.; Van den Mooter, G.; Augustijns, P. Solubility Increases Associated with Crystalline Drug Nanoparticles: Methodologies and Significance. *Mol. Pharmaceutics* **2010**, *7*, 1858–1870.
28. Pasche, S.; De Paul, S. M.; Vörös, J.; Spencer, N. D.; Textor, M. Poly(l-lysine)-graft-poly(ethylene glycol) Assembled Monolayers on Niobium Oxide Surfaces: A Quantitative Study of the Influence of Polymer Interfacial Architecture on Resistance to Protein Adsorption by ToF-SIMS and in Situ OWLS. *Langmuir* **2003**, *19*, 9216–9225.
29. Szela, S.; Avtges, P.; Valluzzi, R.; Winkler, S.; Wilson, D.; Kirschner, D.; Kaplan, D. L. Reduction−Oxidation Control of β-Sheet Assembly in Genetically Engineered Silk. *Biomacromolecules* **2000**, *1*, 534–542.
30. Dado, G. P.; Gellman, S. H. Redox Control of Secondary Structure in a Designed Peptide. *J. Am. Chem. Soc.* **1993**, *115*, 12609–12610.
31. Carampin, P.; Lallana, E.; Laliturai, J.; Carroccio, S. C.; Puglisi, C.; Tirelli, N. Oxidant-Dependent REDOX Responsiveness of Polysulfides. *Macromol. Chem. Phys.* **2012**, *213*, 2052–2061.
32. Mahmoud, E. A.; Sankaranarayanan, J.; Morachis, J. M.; Kim, G.; Almutairi, A. Inflammation Responsive Logic Gate Nanoparticles for the Delivery of Proteins. *Bioconjugate Chem.* **2011**, *22*, 1416–1421.
33. Alexandre, J.; Batteux, F.; Nicco, C.; Chéreau, C.; Laurent, A.; Guillevin, L.; Weill, B.; Goldwasser, F. Accumulation of Hydrogen Peroxide is an Early and Crucial Step for Paclitaxel-Induced Cancer Cell Death Both *in Vitro* and *in Vivo*. *Int. J. Cancer* **2006**, *119*, 41–48.
34. Alexandre, J.; Hu, Y.; Lu, W.; Pelicano, H.; Huang, P. Novel Action of Paclitaxel against Cancer Cells: Bystander Effect Mediated by Reactive Oxygen Species. *Cancer Res.* **2007**, *67*, 3512–3517.
35. Duncan, R.; Gaspar, R. Nanomedicine(s) under the Microscope. *Mol. Pharm.* **2011**, *8*, 2101–2141.
36. Basiruddin, S. K.; Saha, A.; Pradhan, N.; Jana, N. R. Advances in Coating Chemistry in Deriving Soluble Functional Nanoparticle. *J. Phys. Chem. C* **2010**, *114*, 11009–11017.
37. Yu, S.; Scherer, R.; Ortega, R.; Bell, C.; O'Neil, C.; Hubbell, J.; Giorgio, T. Enzymatic- and Temperature-Sensitive Controlled Release of Ultrasmall Superparamagnetic Iron Oxides (USPIOs). *J. Nanobiotechnol.* **2011**, *9*, 7.
38. Mailänder, V.; Landfester, K. Interaction of Nanoparticles with Cells. *Biomacromolecules* **2009**, *10*, 2379–2400.
39. Dubertret, B.; Skourides, P.; Norris, D. J.; Noireaux, V.; Brivanlou, A. H.; Libchaber, A. *In Vivo* Imaging of Quantum Dots Encapsulated in Phospholipid Micelles. *Science* **2002**, *298*, 1759–1762.
40. Fuhrmann, K.; Schulz, J. D.; Gauthier, M. A.; Leroux, J.-C. PEG Nanocages as Non-sheddable Stabilizers for Drug Nanocrystals. *ACS Nano* **2012**, *6*, 1667–1676.
41. Letchford, K.; Liggins, R.; Wasan, K. M.; Burt, H. *In vitro* Human Plasma Distribution of Nanoparticulate Paclitaxel is Dependent on the Physicochemical Properties of Poly(ethylene glycol)-block-Poly(caprolactone) Nanoparticles. *Eur. J. Pharm. Biopharm.* **2009**, *71*, 196–206.